



NLO + parton-shower generator for Wc production in the POWHEG BOX RES

Silvia Ferrario Ravasio^{1,a}, Carlo Oleari^{2,b}

¹ CERN, Theoretical Physics Department, 1211 Geneva 23, Switzerland

² INFN, Sezione di Milano-Bicocca, Università degli Studi di Milano-Bicocca, Piazza della Scienza 3, 20126 Milan, Italy

Received: 9 May 2023 / Accepted: 18 July 2023 / Published online: 31 July 2023
© The Author(s) 2023

Abstract We present the implementation of a next-to-leading-order plus parton-shower event generator for the hadronic production of a heavy charm quark accompanied by a leptonically-decaying W boson in the POWHEG BOX RES framework. We consider both signatures, i.e. $pp \rightarrow c \ell^- \bar{\nu}_\ell$ and $pp \rightarrow \bar{c} \ell^+ \nu_\ell$, and we include exactly off-shell and spin-correlation effects, as well as off-diagonal Cabibbo–Kobayashi–Maskawa contributions. We present particle-level results, obtained interfacing our code with the Herwig7.2 and Pythia8.3 shower Monte Carlo event generators, including hadronization and underlying-event effects, and compare them against the data collected by the CMS Collaboration at $\sqrt{s} = 13$ TeV.

Contents

1	Introduction	1
2	Contributing processes and technical details	2
2.1	The decoupling and $\overline{\text{MS}}$ schemes	4
2.2	Renormalization and factorization scale settings	4
2.3	Numerical inputs	4
2.4	Fixed-order validation	5
3	Details of the POWHEG matching	5
4	NLO + parton-shower results	8
4.1	The POWHEG BOX RES matching with Herwig7.2 and Pythia8.3	9
4.1.1	QTilde shower	9
4.1.2	Dipole shower	9
4.1.3	Vincia shower	10
4.2	NLO + PS results with hadronization and underlying-event effects	10
4.3	Comparison with the CMS data	13

^a e-mail: silvia.ferrario.ravasio@cern.ch

^b e-mail: carlo.oleari@mib.infn.it (corresponding author)

5	Conclusions	13
	References	14

1 Introduction

The production of a W boson in association with a charm quark (c), tagged by the full reconstruction of the charmed D hadron from the clear experimental signature of its decay products, is one of the main probe of the strange-quark content of the colliding particles at a hadron collider, such as the LHC. In fact, the leading contribution to Wc production (W^-c and $W^+\bar{c}$) comes from the scattering of a strange quark (s or \bar{s}) and a gluon, from the two incoming hadrons, since the corresponding Cabibbo–Kobayashi–Maskawa (CKM) matrix element is the dominant one for this channel. The two leading-order (LO) Feynman diagrams for Wc production are depicted in Fig. 1.

As first illustrated in Ref. [1], this process can be used to put constraints on the strange-quark content of the colliding hadrons, i.e. protons at the Large Hadron Collider (LHC). Several measurements of Wc production have already been performed at the LHC as it went through the increasing energy upgrade from 7 to 13 TeV, by the ATLAS [2,3], the CMS [4–6] and the LHCb Collaborations [7].

The next-to-leading order (NLO) QCD cross section for Wc production has been known for a while, and studied both at the Tevatron [8] and at the LHC [9]. More recently, the complete set of next-to-next-to-leading order (NNLO) QCD corrections to the dominant CKM-diagonal contribution have been computed in Ref. [10] and further extended with full CKM dependence, including the dominant NLO electro-weak corrections, in Ref. [11], in the massless-charm limit.

The first dedicated NLO QCD + PS generator for Wc production was done in Ref. [12], within the PowHe1 event

generator, based on the POWHEG method [13], with the W boson decaying leptonically, including charm-quark mass effects in the hard-scattering matrix elements and a non-diagonal CKM matrix.¹

In this paper we describe the implementation of a NLO + parton-shower generator for the hadro-production of a massive charm quark accompanied by a leptonically-decaying W boson in the POWHEG BOX RES framework [17–19]. We include exactly off-shell and spin-correlation effects, as well as off-diagonal CKM contributions.

The POWHEG BOX RES framework is able to deal with radiation off resonances. Although for the case at hand of QCD corrections to a leptonically decaying W boson, the machinery of radiation off resonances is not necessary, since no QCD radiation can be emitted from the leptons, we have implemented Wc production in this framework for several reasons:

1. Better handling of final-state radiation from heavy quarks, as radiation collinear to heavy partons is dealt with an appropriate importance sampling.²
2. The future inclusion of NLO electro-weak corrections is facilitated, since the process is already in the right framework to deal with photon radiation, not only from quarks, but also from the charged lepton in the W decay, where the virtuality of the resonance has to be preserved during the generation of the hardest radiation performed by the POWHEG BOX RES.
3. All the processes for which the NNLO+PS accuracy has been reached [21–24] using the MiNNLO_{PS} formalism [25,26] are implemented in the POWHEG BOX RES framework. It would then be easier to implement also the NNLO QCD corrections to Wc production in this framework too.

The paper is organized as follows. In Sect. 2 we give some technical details about the process we are studying at LO and NLO, we describe the change of scheme of our calculation and the default choice of the renormalization and factorization scales that we have used. In addition we give the numerical value of the input parameters we have used in our simulation, and we present the validation of the fixed-order NLO results. In Sect. 3 we give details of the matching of the NLO amplitudes with the POWHEG method, as implemented in the POWHEG BOX RES framework. We discuss the effects

¹ Predictions for Wc hadro-production, at NLO QCD accuracy, matched to PS, according to the MC@NLO matching framework [14], can also be obtained using the MadGraph5_aMC@NLO framework [15]. In addition, one can also use the automatic interface between the POWHEG BOX and MadGraph5_aMC@NLO [16] to build the code, according to the POWHEG matching framework.

² The first treatment of radiation from heavy parton in the POWHEG BOX appeared in Ref. [20].

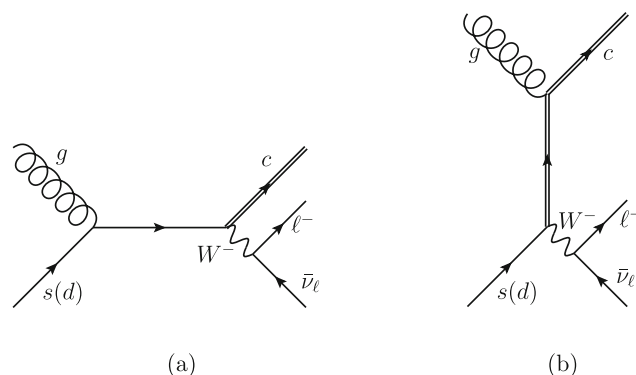


Fig. 1 Feynman diagrams contributing to the partonic process $g s(d) \rightarrow \ell^- \bar{\nu}_\ell c$ at LO, in the s channel (a), on the left, and t channel (b), on the right. The heavy charm quark is represented as a double line

of the extra degrees of freedom offered by this matching and their numerical impact. In Sect. 4 we present a few interesting kinematic distributions computed with events obtained by completing the first radiation emission performed by the POWHEG BOX RES code, with three showering models, implemented in Herwig7.2 and Pythia8.3, and we discuss the differences. We also present results with full hadronization in place and in the presence of underlying events, and we compare them with the experimental data collected by the CMS Collaboration at 13 TeV.

The POWHEG BOX RES framework, together with the Wc generator, can be downloaded at <http://powhegbox.mib.infn.it>.

2 Contributing processes and technical details

In this section we discuss the implementation of the processes $pp \rightarrow \ell^- \bar{\nu}_\ell c$ and $pp \rightarrow \ell^+ \nu_\ell \bar{c}$ at NLO QCD accuracy.

We consider the c quark to be massive, with all the other lighter quarks and anti-quarks treated as massless. At LO, the partonic subprocesses that contribute to Wc production are

$$\begin{aligned}
 g d &\rightarrow \ell^- \bar{\nu}_\ell c \\
 g s &\rightarrow \ell^- \bar{\nu}_\ell c \\
 g \bar{d} &\rightarrow \ell^+ \nu_\ell \bar{c} \\
 g \bar{s} &\rightarrow \ell^+ \nu_\ell \bar{c}
 \end{aligned} \tag{2.1}$$

where the channels involving a down (anti-)quark are Cabibbo-suppressed with respect to those containing the strange (anti-)quark. We are neglecting contributions arising from a bottom quark in the initial state: these contributions are suppressed both by the bottom parton distribution function (PDF), and also by the smallness of the CKM matrix element $|V_{cb}|$.

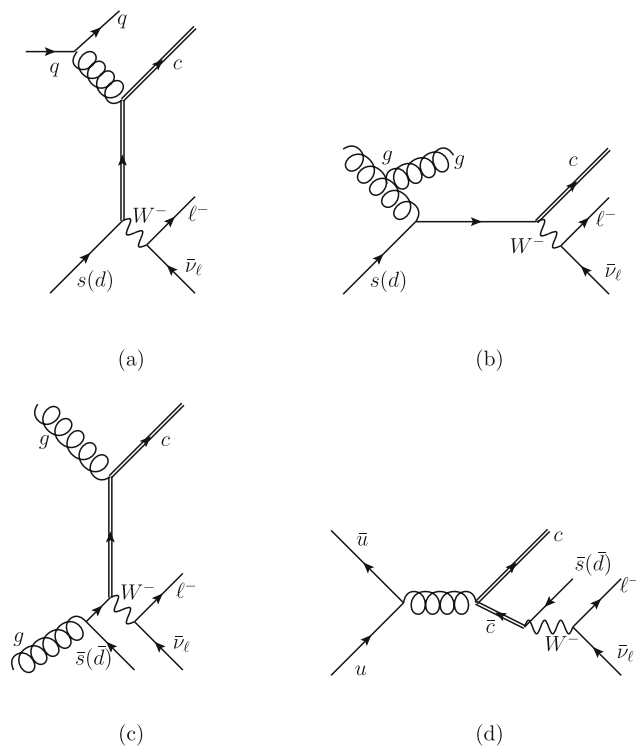


Fig. 2 Examples of Feynman diagrams contributing to the real corrections for the process $pp \rightarrow \ell^- \bar{\nu}_\ell c j$, where $j = g, u, d, s, \bar{u}, \bar{d}, \bar{s}$. The last Feynman diagram (d) is an example of “regular” contribution, i.e. no singularities are associated with this process

The tree-level Feynman diagrams contributing to the process $g s(d) \rightarrow \ell^- \bar{\nu}_\ell c$ are represented in Fig. 1: this process can proceed either via an s -channel exchange of a $s(d)$ quark (left panel), or via a t -channel exchange of a c quark (right panel). The mass of the charm quark ensures that the latter contribution is finite also when its transverse momentum is vanishing.

In the following we discuss only W^- production, since a similar discussion is also valid for W^+ production, after charge conjugation of the involved subprocesses.

Together with the QCD virtual corrections to the subprocesses in Eq. (2.1), not depicted here, also the real corrections contribute at the next-to-leading order. Examples of Feynman diagrams contributing to the real corrections for the process $pp \rightarrow \ell^- \bar{\nu}_\ell c j$ are shown in Fig. 2. We can separate the real-correction contributions into two classes:

1. The corrections of the type $pp \rightarrow \ell^- \bar{\nu}_\ell c j$, with $j = g, u(\bar{u}), d(\bar{d}), s(\bar{s})$, that are singular in the limit of the unresolved jet

$$\begin{aligned}
 q(\bar{q}) s(d) &\rightarrow \ell^- \bar{\nu}_\ell c q(\bar{q}) \\
 g s(d) &\rightarrow \ell^- \bar{\nu}_\ell c g \\
 g g &\rightarrow \ell^- \bar{\nu}_\ell c \bar{s}(d),
 \end{aligned}
 \tag{2.2}$$

where $q = u, d, s$. Examples of these contributions are depicted in Fig. 2, diagrams (a), (b) and (c). We will refer to these terms with R in the following.

2. The corrections of the type

$$q \bar{q} \rightarrow \ell^- \bar{\nu}_\ell c \bar{q}',
 \tag{2.3}$$

where $q = u, d, s$ and $q' = s, d$, which do not have any singularities associated with the extra light-parton emission, and are called regular, in the POWHEG jargon and will be indicated with R_{reg} . Again we do not consider contributions with a final-state b quark. An example of this type of contributions is depicted in Fig. 2d.

Notice that the square of the diagrams contributing to the regular processes (Fig. 2d), as well as similar diagrams with two gluons in the initial state (that interfere with the one in (c)), suffer from another potential source of divergence, due to the presence of the charm anti-quark in the s channel. In fact, when the invariant mass of the system comprising the $\bar{s}(\bar{d})$ quark and the two leptons is equal to the charm mass m_c , these diagrams are divergent, due to the fact that the c -quark propagator goes on shell. In order to avoid this singularity, we can impose a technical cut on the invariant mass of the off-shell W boson

$$m_{\ell\nu}^2 \equiv (p_\ell + p_\nu)^2 > m_c^2,
 \tag{2.4}$$

in the theoretical simulation. In order to make a closer contact to experimentally accessible quantities, a more realistic cut is in general imposed on the transverse mass of the W system, m_{TW} , defined as

$$m_{TW}^2 = 2 p_{\perp\ell} p_{\perp\nu} (1 - \cos \Delta\varphi),
 \tag{2.5}$$

where $\Delta\varphi$ is the azimuthal separation between the transverse momenta of the charged lepton and the missing energy of the neutrino.

We neglect contributions with two charmed quark in the final state, such as $\bar{u}d \rightarrow \ell^- \bar{\nu}_\ell c \bar{c}$, coming from the splitting $g \rightarrow c \bar{c}$, since these contributions are subtracted from experimental data in studies aimed at extracting information on the strange-quark parton distribution function, as illustrated in Sect. 4.2.

The Born and virtual matrix elements, as well as the Born colour- and spin-correlated amplitudes, necessary to the POWHEG BOX RES to automatically implement the POWHEG formalism, have been computed analytically.³ The one-loop amplitudes have been validated against the Gosam code [27,28]. The matrix elements for the real contributions were instead generated using Madgraph4 [29] and its interface with the POWHEG BOX [30].

³ In fact, the analytic calculation of these amplitudes was part of the Master thesis of one of the authors.

2.1 The decoupling and $\overline{\text{MS}}$ schemes

When performing a fixed-order calculation with massive quarks, one can define at least two consistent renormalization schemes that describe the same physics: the usual $\overline{\text{MS}}$ scheme, where all flavours are treated on equal footing, and a mixed scheme [31], called decoupling scheme [32], in which the n_f light flavours are subtracted in the $\overline{\text{MS}}$ scheme, while the heavy-flavour loop is subtracted at zero momentum. In this scheme, the heavy flavour decouples at low energies. This is the scheme we have used in the renormalization of our analytic calculation, with $n_f = 3$.

If the decoupling scheme is chosen, then the strong coupling constant α_s runs with three light flavours, and the parton distribution functions should not include the charm quark in the evolution.

To make contact with other results expressed in terms of the $\overline{\text{MS}}$ strong coupling constant, running with five light flavours, and with PDFs with five flavours, we prefer to change our renormalization scheme and to switch to the $\overline{\text{MS}}$ one. The procedure for such a switch is well known, and was discussed in Ref. [33]. This procedure, applied to the b quark, is also illustrated in Appendix A of Ref. [34].

For the case under study, since the LO process contains only one power of α_s , if we want to express our calculation in terms of a coupling constant defined in the $\overline{\text{MS}}$ scheme with five active flavours, we need to add the following contribution to the cross section

$$\Delta V_{\alpha_S}(\mu_R; m_b, m_c) = -\frac{1}{3} T_F \frac{\alpha_S}{\pi} \left(\log \frac{\mu_R^2}{m_c^2} + \log \frac{\mu_R^2}{m_b^2} \right) B, \quad (2.6)$$

where B is the Born cross section, m_b the bottom mass and μ_R is the renormalization scale. A corresponding modification has to be applied if we want to employ PDFs with five active flavours. The gluon PDF, which appears in the LO cross section, induces a correction

$$\Delta V_g(\mu_F; m_b, m_c) = +\frac{1}{3} T_F \frac{\alpha_S}{\pi} \left(\log \frac{\mu_F^2}{m_c^2} + \log \frac{\mu_F^2}{m_b^2} \right) B, \quad (2.7)$$

where μ_F is the factorization scale. The quark PDF receives only corrections that starts at order α_s^2 , and can thus be neglected. By adding Eqs. (2.6) and (2.7), we get the conversion factor for the two schemes

$$\Delta V(\mu_F, \mu_R) = \Delta V_{\alpha_S} + \Delta V_g = \frac{2}{3} T_F \frac{\alpha_S}{\pi} B \log \frac{\mu_F^2}{\mu_R^2}, \quad (2.8)$$

that turns out to be independent from the bottom and charm masses, and different from zero only if the renormalization and factorization scales are different.

2.2 Renormalization and factorization scale settings

In the POWHEG BOX there is the option to use a different renormalization and factorization scale when computing the real contribution (and/or the subtraction terms, i.e. their soft and collinear limits) or the Born and the virtual ones. The only requirement is that the scale used in the evaluation of the real contributions (and possibly of the subtraction terms) must tend to the scale used in the Born amplitude, when the emitted parton gets unresolved.

The default central scale used in our simulation in the evaluation of the Born, virtual, real and subtraction terms is

$$\mu = \frac{H_T}{2} \quad (2.9)$$

with

$$H_T = \sqrt{|\vec{p}_{\perp c}|^2 + m_c^2} + \sqrt{|\vec{p}_{\perp \ell} + \vec{p}_{\perp \nu}|^2 + (p_\ell + p_\nu)^2}, \quad (2.10)$$

evaluated with the kinematics of the underlying-Born configuration. The regular real term R_{reg} has no underlying Born configuration, and the scale H_T is computed using the kinematics of the real emission contribution, adding also the transverse momentum of the massless emitted parton.

$$H_T = \sqrt{|\vec{p}_{\perp c}|^2 + m_c^2} + \sqrt{|\vec{p}_{\perp \ell} + \vec{p}_{\perp \nu}|^2 + (p_\ell + p_\nu)^2} + |\vec{p}_{\perp j}|. \quad (2.11)$$

Other options contemplate the use of the scale (2.11) also in the real term and/or in the subtraction terms,⁴ or a fixed scale,⁵ such as $\mu = m_W$.

The renormalization and factorization scales, μ_R and μ_F , are defined multiplying μ by the factors ξ_R and ξ_F respectively. The uncertainty due to missing higher order corrections is estimated considering the 7-point scale variations

$$(\xi_R, \xi_F) = (1, 1), (1, 2), (1, 0.5), (2, 1), (0.5, 1), (2, 2), (0.5, 0.5). \quad (2.12)$$

We employ the NNPDF3.1_nlo_pdfas [35,36] PDF set, which is also used to determine the running of the strong coupling.⁶

2.3 Numerical inputs

We have simulated Wc production in pp collisions at $\sqrt{s} = 13$ TeV. The input parameters we have used are

$$m_W = 80.385 \text{ GeV} \quad \Gamma_W = 2.085 \text{ GeV}$$

⁴ This option can be chosen adding the flags `btlscale_real 1` and/or `btlscale_ct 1` in the input card.

⁵ Set `runningscales 0` in the input card.

⁶ This option can be selected by adding the flag `alphas_from_pdf 1` in the input card. Otherwise the running of α_s is computed at two loops internally by the POWHEG BOX RES.

$$m_Z = 91.1876 \text{ GeV} \quad \Gamma_Z = 2.4952 \text{ GeV} \quad (2.13)$$

$$G_\mu = 1.16639 \times 10^{-5} \text{ GeV}^{-2} \quad m_c = 1.5 \text{ GeV}.$$

The electromagnetic coupling is obtained in the G_μ scheme

$$\alpha_{\text{em}} = \frac{\sqrt{2}}{\pi} G_\mu m_W^2 \left(1 - \frac{m_W^2}{m_Z^2} \right), \quad (2.14)$$

and the values of relevant CKM matrix elements are

$$|V_{cd}| = 0.22438, \quad |V_{cs}| = 0.97356. \quad (2.15)$$

In our calculation we have neglected the mass of the leptons. Only at the stage of event generation a leptonic mass is assigned to the charged lepton once the full kinematics of the event is generated.⁷ The assignment of the mass is done through a reshuffling procedure that preserves the total energy and momentum, and the virtuality of the resonances. The values of the lepton masses we have used are given by

$$m_e = 0.511 \times 10^{-3} \text{ GeV},$$

$$m_\mu = 0.1057 \text{ GeV}, \quad m_\tau = 1.777 \text{ GeV}. \quad (2.16)$$

Furthermore, following the discussion that precedes Eq. (2.4), we always apply a technical loose cut, at the generation stage, on the W -boson virtuality

$$m_{\ell\nu} > 2 \text{ GeV}. \quad (2.17)$$

2.4 Fixed-order validation

In this section we compare our fixed-order results with those obtained with the MCFM code [37,38]. In order to perform the comparison we employ a fixed renormalization and factorization scale set to

$$\mu_F = \mu_R = m_W. \quad (2.18)$$

As we are setting $\mu_F = \mu_R$, the term ΔV defined in Eq. (2.8) vanishes and there is no correction factor. We define the fiducial cross section imposing the following cuts on the transverse momentum and rapidity of the charged lepton, as well on the transverse momentum of the charm quark

$$|\vec{p}_{\perp\ell}| > 26 \text{ GeV}, \quad |y_\ell| < 2.4, \quad |\vec{p}_{\perp c}| > 5 \text{ GeV}. \quad (2.19)$$

These cuts corresponds to the ones employed by the CMS Collaboration to define the inclusive cross section in the analysis described in Ref. [6] at $\sqrt{s} = 13 \text{ TeV}$.

As discussed in Sect. 2, around Eqs. (2.4) and (2.5), in order to avoid the charm-propagator singularity in diagrams like the one in Fig. 2d, we also implement a cut on the transverse mass of the W system

$$m_{TW} > 20 \text{ GeV}. \quad (2.20)$$

⁷ The user can also choose in which leptonic family/families the W boson decays, by selecting the value of the flag `vdecaymode` in the input card.

In Table 1 we show the integrated cross section at LO and NLO obtained with our code and with MCFM. In all cases a sub-permille agreement is found. Good agreement is found also at the differential level, as it can be seen in Fig. 3, where we illustrated the transverse mass of the reconstructed W boson (left panel) and the transverse momentum of the charmed quark (right panel).

3 Details of the POWHEG matching

In this section we briefly recall the expression for the differential cross section generated with the POWHEG method [13] for the process under consideration, focusing for simplicity only on the $pp \rightarrow \ell \bar{\nu}_\ell c$ signature, in order to discuss further sources of theoretical uncertainty intrinsic to the POWHEG method.

The NLO cross section reads

$$d\sigma_{\text{NLO}} = B(\Phi_3; \mu_R, \mu_F) d\Phi_3 + \frac{\alpha_S(\mu_R)}{2\pi} [V(\Phi_3; \mu_R, \mu_F) d\Phi_3 + R(\Phi_{3+1}; \mu_R, \mu_F) d\Phi_{3+1} + R_{\text{reg}}(\Phi_{3+1}; \mu_R, \mu_F) d\Phi_{3+1}], \quad (3.1)$$

where B , V , R and R_{reg} are the Born, virtual, real and regular real matrix elements, multiplied by the appropriate PDF and flux factors. As stated in Sect. 2, we indicate with R_{reg} the terms arising from the flavour configurations of Eq. (2.3), which do not contain any QCD singularity, while the processes in Eq. (2.2) are designated with R . The Born and virtual cross sections are evaluated using a three-body phase space Φ_3 , while, in the real contributions, an additional light parton is present. The matrix elements depend on the μ_R scale, as the LO starts with one power of the strong coupling constant α_S , while the μ_F dependence arises from the incoming-parton PDFs. To build the POWHEG cross section, the real term R is split into a singular R_s and a finite contribution R_f , and the \bar{B} term is defined as

$$\bar{B}(\Phi_3; \mu_F, \mu_R) = B(\Phi_3; \mu_R, \mu_F) + \frac{\alpha_S(\mu_R)}{2\pi} \left[V(\Phi_3; \mu_R, \mu_F) + \int d\Phi_1 R_s(\Phi_{3+1}; \mu_R, \mu_F) \right], \quad (3.2)$$

where Φ_1 is the radiation phase space, defined in terms of three radiation variables. The probability of not having any resolved emissions up to a scale k'_T is given by

$$\Delta_s(k'_T; \Phi_3) = \exp \left[- \int d\Phi_1 \theta[k_T(\Phi_1) - k'_T] \frac{\alpha_S(k_T)}{2\pi} \frac{R_s(\Phi_{3+1}; k_T, k_T)}{B(\Phi_3; k_T, k_T)} \right], \quad (3.3)$$

Table 1 Fiducial cross section obtained with MCFM and our generator (PWG RES) for the processes $pp \rightarrow e^- \bar{\nu}_e c$ and $e^+ \nu_e \bar{c}$ at LO (left columns) and NLO (right columns) at $\sqrt{s} = 13$ TeV within the fiducial

cuts of Eqs. (2.19) and (2.20), with $\mu_F = \mu_R = m_W$. The input parameters are discussed in Sect. 2.3. In the last row we show the ratio between the MCFM and the POWHEG BOX RES predictions

σ [fb]	$e^- \bar{\nu}_e c$ @ LO	$e^+ \nu_e \bar{c}$ @ LO	$e^- \bar{\nu}_e c$ @ NLO	$e^+ \nu_e \bar{c}$ @ NLO
PWG RES	352.7(1)	341.1(1)	497.2(2)	480.8(2)
MCFM 10	352.9(2)	341.2(2)	497.0(2)	481.0(3)
Ratio	1.0005(5)	1.0002(5)	0.9996(7)	1.0004(7)

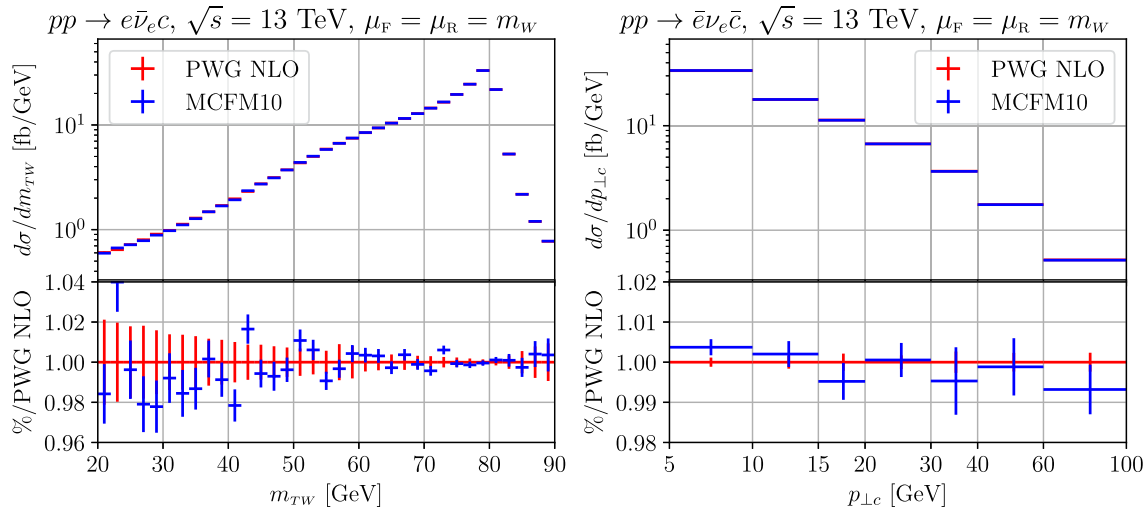


Fig. 3 Differential distribution for the transverse mass of the reconstructed W^- boson for the processes $pp \rightarrow e^- \bar{\nu}_e c$ (left) and the transverse momentum of the heavy anti-charm quark for the processes $pp \rightarrow e^+ \nu_e \bar{c}$ (right) at NLO accuracy. The input parameters are

discussed in Sect. 2.3. The ratio between predictions obtained with MCFM (blue) and the POWHEG BOX RES (red) is also shown. The statistical error bars from the Monte Carlo integrator are also shown

where the factorization and the renormalization scales are evaluated at the scale k_T , which corresponds to the transverse momentum of the light parton, if it is collinear to an initial-state parton, while, for gluon emissions from the final-state charm quark, it is given by

$$k_T^2 = 2 \frac{E_g}{E_c} (p_g \cdot p_c), \tag{3.4}$$

where p_g and p_c are the gluon and charm four-momenta and E_g and E_c their energies in the partonic center-of-mass frame.

The POWHEG cross section finally reads

$$\begin{aligned}
 d\sigma_{\text{PWG}} = & \bar{B}(\Phi_3; \mu_F, \mu_R) d\Phi_3 \left[\frac{\alpha_s(k_T)}{2\pi} \frac{R_s(\Phi_{3+1}; k_T, k_T)}{B(\Phi_3; k_T, k_T)} \right. \\
 & \left. \Delta_s(k_T; \Phi_3) d\Phi_1 + \Delta_s(k_T^{\text{min}}; \Phi_3) \right] \\
 & + \frac{\alpha_s(\mu_R)}{2\pi} R_f(\Phi_{3+1}; \mu_R, \mu_F) d\Phi_{3+1} \\
 & + \frac{\alpha_s(\mu_R)}{2\pi} R_{\text{reg}}(\Phi_{3+1}; \mu_R, \mu_F) d\Phi_{3+1}, \tag{3.5}
 \end{aligned}$$

where k_T^{min} is an infrared cutoff.

There are several degrees of freedom in the implementation of Eq. (3.5). One of them is in the choice of the renormalization and factorization scales μ_R and μ_F in the R_f and R_{reg} terms, as well as in the term R_s appearing in \bar{B} in Eq. (3.2), as discussed in Sect. 2.2. Another one is in the choice of how to separate R into a singular part R_s and a finite one R_f . Without loss of generality, one can separate the two contributions introducing what is called a “damping function”, $f(k_T)$, that satisfies

$$0 \leq f(k_T) \leq 1, \quad \lim_{k_T \rightarrow 0} f(k_T) = 1 \tag{3.6}$$

and define

$$R_s = f(k_T) R, \quad R_f = [1 - f(k_T)] R. \tag{3.7}$$

For the process we are studying, we have considered two different forms for f

$$f_1(x) = \frac{1}{1 + x^2} \tag{3.8}$$

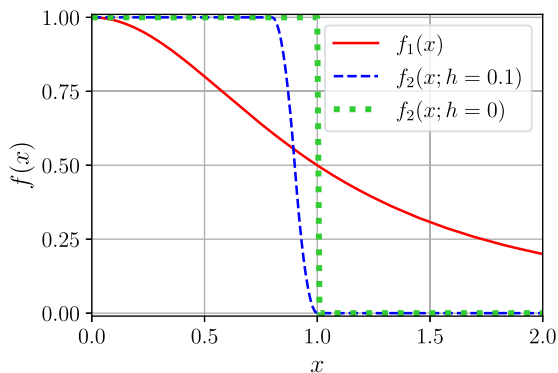


Fig. 4 Comparison of three damping functions used to separate the real contribution into a singular and a finite part, as detailed in Sect. 3

$$f_2(x; h) = \begin{cases} 1 & \text{for } x \leq 1 - 2h \\ 1 - \frac{(1 - 2h - x)^2}{2h^2} & \text{for } 1 - 2h < x \leq 1 - h \\ \frac{(1 - x)^2}{2h^2} & \text{for } 1 - h < x \leq 1 \\ 0 & \text{for } x > 1, \end{cases} \tag{3.9}$$

with

$$x = \frac{1}{\mu} \sqrt{k_T^2 - m_c^2} \theta(k_T - m_c), \tag{3.10}$$

where μ is defined in Eq. (2.9), and $0 \leq h \leq 1/2$ is a free parameter. The value of x is set to 0 if $k_T < m_c$, so that no finite contribution is present with k_T below the charm mass.⁸ The functional form f_2 in Eq. (3.9), with $h = 0.3$, is the default damping function in the Herwig7.2 event generator [39], while f_1 in Eq. (3.8) corresponds to the default option of the POWHEG BOX RES. In Fig. 4 we provide a graphical representation of f_1 , $f_2(h = 0.1)$ and $f_2(h = 0)$.⁹

In the following we investigate the dependence of several inclusive (with respect to the QCD radiation) observables, such as the leptonic observables and the rapidity and the transverse momentum of the jet containing the charm quark.

We reconstruct jets using the Fastjet [40] implementation of the anti- k_T algorithm [41] with $R = 0.5$.¹⁰ To this aim,

⁸ In the POWHEG BOX RES, no damping factor is applied when the emitter is massive.

⁹ Furthermore, the code has by default the Bornzerodamp flag activated. This provides a way to deal with kinematic configurations where the real contribution is too large with respect to its soft and collinear limits, signalling that the kinematics of the underlying Born gives rise to a Born amplitude that is particularly small, i.e. close to zero. See Ref. [18] for more details.

¹⁰ There are no infrared-safety issues related to the definition of a flavoured jet since we are dealing with massive quarks, and the charm mass prevents any divergence. For a discussion on this subject, see for example, Ref. [42].

Table 2 Setups for the implementation of the POWHEG cross section given in Eq. (3.5). The second column denotes the kinematic configuration used to evaluate the renormalization and factorization scales in the computation of the real and subtraction terms, while the last column shows which profile function is used to evaluate Eq. (3.7). The functional forms of f_1 and f_2 are given in Eqs. (3.8) and (3.9) respectively

Acronym	Scales in R	Damping function f
B ₀	Underlying-Born kinematics	1
B ₁	Underlying-Born kinematics	f_1
B ₂	Underlying-Born kinematics	$f_2(h = 0.1)$
R ₀	Real kinematics	1

we have considered the setups listed in Table 2 to compute the POWHEG cross section given in Eq. (3.5). The central value of the renormalization and factorization scales is set to $H_T/2$ (see Eq. (2.9)).

In the following figures we will compare some kinematic distributions computed with six different setups: two fixed-order NLO results, one computed using the underlying-Born kinematics (NLO_B) for the renormalization and factorization scale in the real contributions, and the other one using the full real-event kinematics, indicated with NLO_R. The other four distributions are computed analysing the POWHEG-generated events at the “Les Houches” (LHE) level, i.e. events with the first hardest radiation generated according to Eq. (3.5), adopting the setup scales and damping functions of Table 2. For inclusive observables, the LHE results should agree with the fixed-order NLO ones up to NNLO terms.

In Fig. 5 we plot the transverse mass of the W boson (left panel) and the rapidity of the charmed jet (right panel). The NLO_B results (blue line) are roughly 3% higher than the NLO_R ones (black line), although always contained in the grey scale-uncertainty band of NLO_R, computed performing the 7-point scale variations in Eq. (2.12). Furthermore, all the distributions at the LHE level agree with the corresponding fixed order calculation, within the scale-variation band.

The transverse momentum of the W boson, $p_{\perp W}$, and of the charmed jet, $p_{\perp jc}$, are illustrated on the left and right panel of Fig. 6, respectively. Comparing the two NLO predictions computed with different scales, one can see that the use of the underlying-Born scales favours a harder spectrum, although the result always lies within the scale-variation band of the NLO_R one, except for the very last bin. This is due to the fact that, for large c -jet transverse momentum, it is quite likely to produce a $c \rightarrow cg$ splitting that enhances the value of H_T . As such, the underlying-Born kinematics yields a lower scale and hence a larger value for α_s , that enhances the cross section. The same behaviour can be seen also at the LHE level.

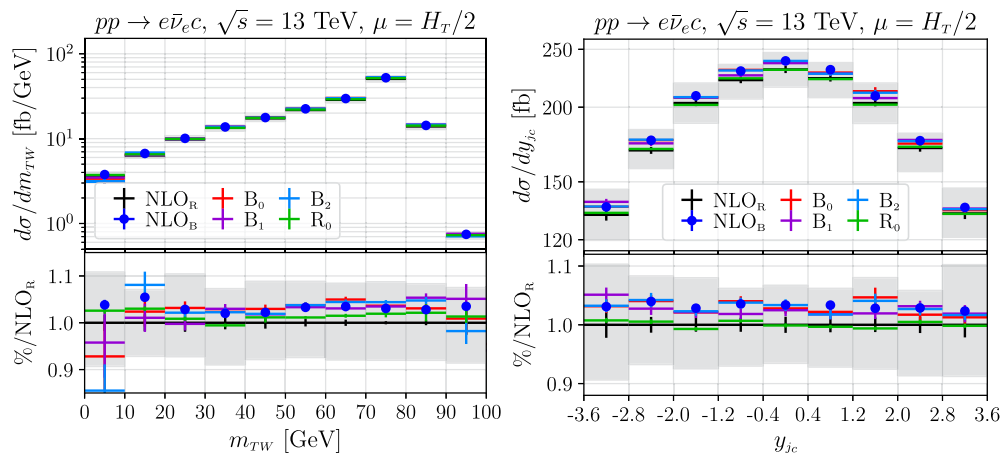


Fig. 5 The transverse mass distribution of the reconstructed W boson (left) and the rapidity of the charmed jet (right) at NLO (NLO_B and NLO_R) and at the Les Houches event level, for the choices of the scales and damping functions listed in Table 2. The grey bands are

obtained performing the 7-point scale variations in Eq. (2.12) of the NLO_R results. The statistical errors from the integration procedure are also shown

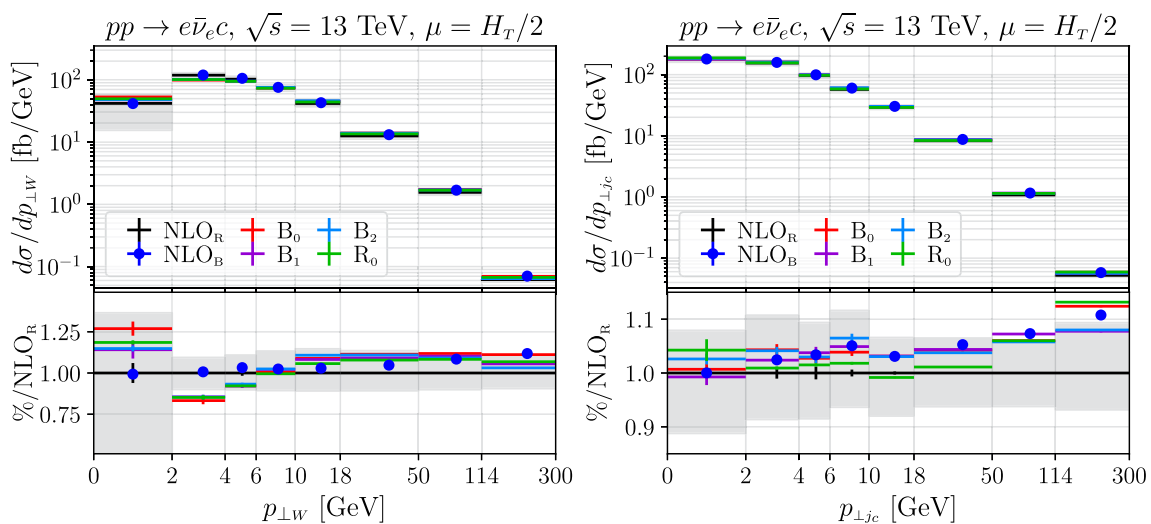


Fig. 6 Same as Fig. 5 but for the transverse momentum of the reconstructed W boson (left) and of the charmed jet (right)

In the experimental analyses, such as the one in Ref. [6], an important role is played by the measurement of the transverse momentum and rapidity of the charged lepton. In Fig. 7 we then plot these quantities, after applying the cuts of Eq. (2.19), that are the same as those used by the CMS Collaboration, as well as a cut on m_{TW} , defined in Eq. (2.20). As far as the fixed-order NLO results is concerned, the NLO_B curves lie a few percent above the NLO_R one, both for the transverse momentum and the rapidity. This is again due to the higher value of α_s when the renormalization scale is evaluated with the underlying-Born kinematics. Differences up to 10% can also be seen among the LHE curves, but, in general, all these curves lie within the grey uncertainty band of the NLO_R result, so that they are consistent among each other.

We thus conclude that no significant differences are found among the several damping factors, particularly when realistic analysis cuts are applied, and that the main theoretical uncertainties arise from scale variations.¹¹

4 NLO + parton-shower results

In this section, we present full results after the completion of the POWHEG shower performed by general-purpose

¹¹ In this analysis we are neglecting the dependence on the PDF set. This topic is addressed in detail by the authors of Refs. [11, 12], which considered several sets, where the charm PDF is intrinsic or dynamically generated. The outcome they found depends on the PDF set used in the simulation: for some sets, the PDF-variation band is smaller than the scale-variation one, for others it is comparable or slightly larger.

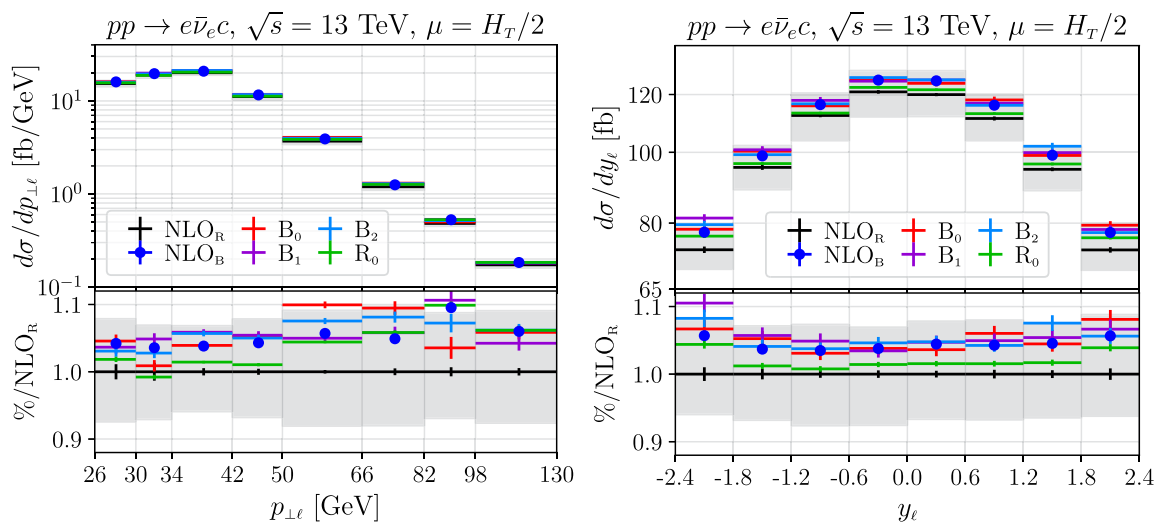


Fig. 7 Same as Fig. 5 but for the transverse momentum (left) and rapidity (right) of the charged lepton, with the cuts in Eqs. (2.19) and (2.20) in place

Monte Carlo (MC) programs, such as Herwig7.2 [43, 44] and Pythia8.3 [45,46], including hadronization and underlying-event effects.

We have showered the Les Houches events that we have produced using the POWHEG BOX RES code, employing the Herwig7.2 angular-ordered shower (that we label as “QTilde” shower), and the default Pythia8.3 shower with fully local recoil [47] (that we denote as “Dipole” shower), as well as the Pythia implementation of the Vincia shower [48,49].

For all the different types of shower we use the default setting of their parameters, and we only change the charm mass to agree with the value we have used to generate the Wc sample (see Eq. (2.13)). In Sect. 4.1 we provide additional details of the showers we have employed, while in Sect. 4.2 we investigate the impact of several ingredients provided by the general-purpose MC generators on the simulation of Wc events. Finally, in Sect. 4.3 we compare our results against the experimental data at $\sqrt{s} = 13$ GeV, taken by the CMS Collaboration.

4.1 The POWHEG BOX RES matching with Herwig7.2 and Pythia8.3

4.1.1 QTilde shower

The relevant parameters to shower the POWHEG-generated events with the QTilde shower are taken from the LHE-POWHEG.in input card distributed in the public release of the Herwig7.2 code. In particular the options

```
set /Herwig/Shower/ShowerHandler:
MaxPtIsMuF Yes
```

```
set /Herwig/Shower/ShowerHandler:
Restrict Phasespace Yes
```

instruct the shower to veto all the emissions with transverse momentum larger than the `scalup` variable, which is the hardness of the POWHEG emission. We set the charm mass to 1.5 GeV

```
set /Herwig/Particle/c:NominalMass
1.5*GeV
set /Herwig/Particle/cbar:NominalMass
1.5*GeV
```

and we switch off the decay of unstable hadrons, in order to analyse more quickly the generated events

```
set LesHouchesHandler:DecayHandler NULL
```

By default, the QTilde shower includes also QED emissions, that can be switched off with the option

```
set /Herwig/Shower/ShowerHandler:
Interactions QCD
```

The running coupling is evaluated at two loops in the Catani–Marchesini–Webber scheme [50], with $\alpha_s^{\text{CMW}}(m_Z) = 0.1186$.

4.1.2 Dipole shower

We also considered the Pythia8.3 implementation of a dipole shower with a fully local recoil [47]

```
SpaceShower:dipoleRecoil = on
```

We employed the `PowhegHooks` class to veto emissions harder than the POWHEG one, all the options correspond to the default ones, present in the `main31.cmd` input card

in the public release of the Pythia8.3 code. To generate only the QCD shower, we set

```
SpaceShower:QEDshowerByQ = off
SpaceShower:QEDshowerByL = off
TimeShower:QEDshowerByQ = off
TimeShower:QEDshowerByL = off
TimeShower:QEDshowerByGamma = off
TimeShower:QEDshowerByOther = off
```

and the hadrons decay is turned off with the flag

```
HadronLevel:Decay = off
```

The running coupling is evaluated at one loop in the $\overline{\text{MS}}$ scheme, and $\alpha_s^{\overline{\text{MS}}}(m_Z) = 0.140$.

4.1.3 Vincia shower

At difference with respect to the Dipole shower, Vincia is an antenna shower. To use its implementation in Pythia8.3, we set

```
PartonShowers:model = 2
```

To properly include charm-mass effects, one has to include the option

```
Vincia:nFlavZeroMass = 3
```

as, by default, this number is set to 4, meaning that only top and bottom are treated as massive. The QED shower can be turned off with the option

```
Vincia:ewMode = 0
```

The running coupling is evaluated at two loops in the Catani–Marchesini–Webber scheme, and $\alpha_s^{\text{CMW}}(m_Z) = 0.127$. Also in this case, we use the PowHegHooks class to avoid to generate emissions harder than the POWHEG one and we do not include the unstable hadrons decay in our simulation.

4.2 NLO + PS results with hadronization and underlying-event effects

In this section we discuss the impact of the parton shower, of the hadronization and of the underlying events on the results generated using our simulation in the POWHEG BOX RES. The results presented in this section do not include the QED shower.

We focus on the $\mu^+ \nu_\mu \bar{c}$ signature at $\sqrt{s} = 13$ TeV. We use the values of the parameters described in Sect. 2.3, and the B₂ setting of Table 2, i.e. the central values for the renormalization and factorization scales are computed using the underlying-Born kinematics, according to Eq. (2.10), and as damping function we use the f_2 profile function of Eq. (3.9) with $h = 0.1$.

We begin by analyzing the effect of the parton shower on the POWHEG BOX distributions (PWG). If, at the end of the shower, an event contains more than one muon (or anti-muon) passing the charged leptonic cuts, only the hardest one is considered to reconstruct the W kinematics.

Since the aim of our analysis is to enhance the sensitivity of the measured cross section to the strange quark PDF, we proceed as follows: if more than one c quark or charmed hadron is present, they are all considered, with the exception of hadrons containing a $c\bar{c}$ pair, which are counted as not charmed. In addition, when in an event the charmed-quark and the muon charges have the same sign (SS), the weight of the event is subtracted from the differential cross sections, while, when they have opposite sign (OS), the weight is added. This procedure effectively removes the background due to events where the final-state charm comes from gluon splitting $g \rightarrow c\bar{c}$, and not from an initial-state strange quark emitting a W boson. Charmed quarks originated from the gluon splitting have the same probability to be SS or OS, so their contribution cancels, when the above procedure is applied.

Jets are reconstructed using the anti- k_T algorithm with $R = 0.5$. The charm content of a jet is defined as $N_c - N_{\bar{c}}$, being $N_c(N_{\bar{c}})$ the number of $c(\bar{c})$ quarks clustered in the jet, and the event weight that we use to fill a jet-related distribution is further weighted by the factor $\pm(N_c - N_{\bar{c}})$, where we use the + sign when the muon has negative charge, and the – sign otherwise.

In the following, we consider both inclusive results (with the technical cut on the W boson virtuality of Eq. (2.17) always in place), as well as more exclusive ones, where we apply the following acceptance cuts

$$|\eta_\mu| < 2.4, \quad p_{\perp\mu} > 26 \text{ GeV}, \\ m_{TW} > 20 \text{ GeV}, \quad |\eta_c| < 2.4, \quad p_{\perp c} > 5 \text{ GeV}, \quad (4.1)$$

used by the CMS Collaboration in their analyses.

At the inclusive level, the parton shower acts non-trivially on the transverse-momentum distribution of the charm quark and of the charmed jet, as portrayed in Fig. 8. In particular, one can notice that the hard tail is depleted, and the region around 5 GeV is instead increased. The effect is milder for the c -jet, as radiation inside the cone with jet radius $R = 0.5$ is still collected in the jet, but more evident for the hadron: in fact, in the high transverse-momentum region, the ratio of the LHE results with the showered ones reaches values around 50% for the quark/hadron, and 10% for the charmed jet.

In order to be able to compare theoretical predictions with data, we also have to include hadronization corrections and the simulation of the underlying-event (UE) production. In Figs. 9 and 10 we illustrate their effect on the NLO+PS distributions obtained with the Herwig7.2 QTilde shower, in Fig. 9, and with the Pythia8.3 Dipole shower, in Fig. 10.

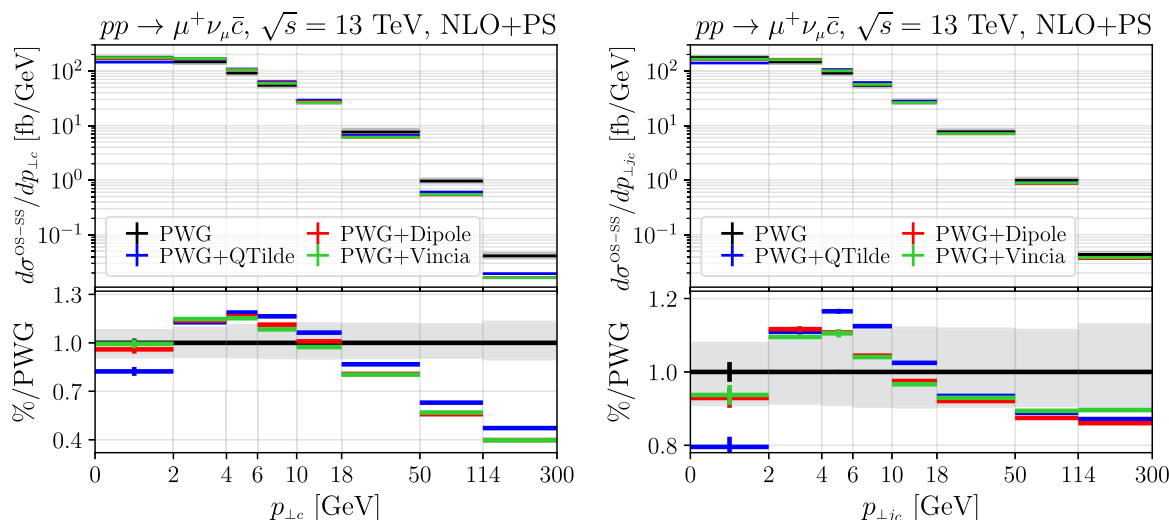


Fig. 8 Effect of three different parton showers (QTilde in blue, Dipole in red and Vincia in green) on the events produced with the POWHEG BOX RES (PWG), in black, for the transverse momentum of the

charmed quark (left panel) and of the charmed jet (right panel), for inclusive cuts. The grey band corresponds to the scale variations of the PWG distribution

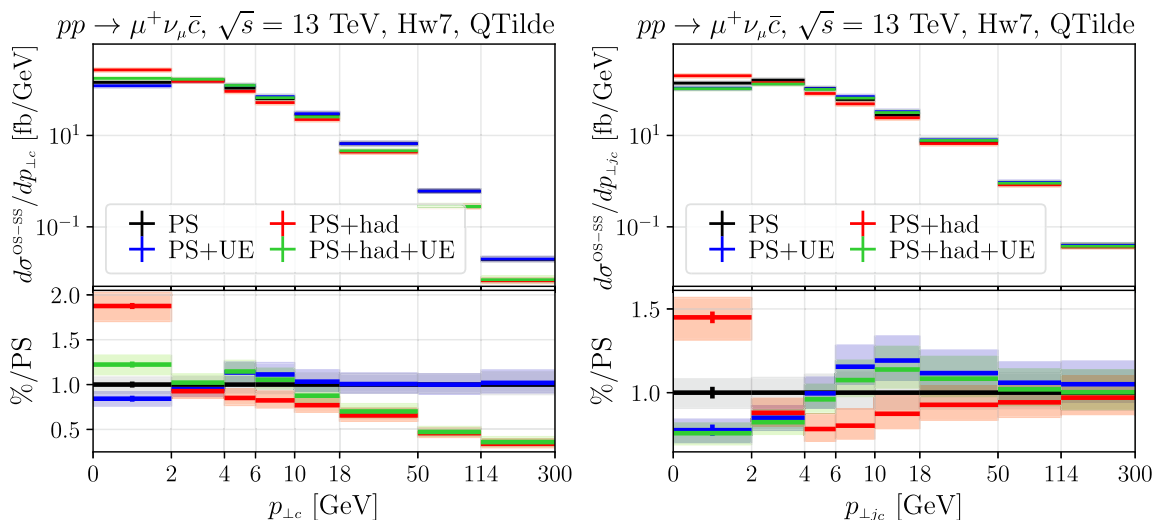


Fig. 9 Effect of the underlying event (UE) and of the hadronization (had) on the NLO+PS distributions obtained with the Herwig7.2 QTilde shower for the transverse-momentum distribution of the charmed quark (left panel) and of the charmed jet (right panel) for

inclusive cuts. The grey band corresponds to renormalization- and factorization-scale variation, obtained using the standard reweighting procedure implemented in the POWHEG BOX RES framework

In all cases we notice that the UE have a small impact on the charmed-quark distribution, except in the region $p_{\perp c} < 10$ GeV. On the other hand, the underlying event hardens the c -jet distribution as it provides further particles that can be clustered in the jet. Hadronization corrections are large (up to 50%) and they soften the p_{\perp} of the charmed quark/hadron. Similar, but milder effects are seen for the charmed jet.

In Fig. 11 we then compare the full simulations obtained with Herwig7.2 and Pythia8.3 against the PWG standalone results. With the exception of the very low transverse-

momentum region, Herwig7.2 and Pythia8.3 distributions are in very good agreement. In particular we notice that now the charmed-hadron distributions, obtained with all the three showers, are essentially indistinguishable for $p_{\perp c} > 10$ GeV, while in Fig. 8 the Herwig7.2 result was quite different from the Pythia8.3 ones. The improved agreement at the particle level is not unexpected, as the results without the inclusion of the hadronization are very sensitive to the shower cutoff, which is tuned alongside the hadronization parameters.

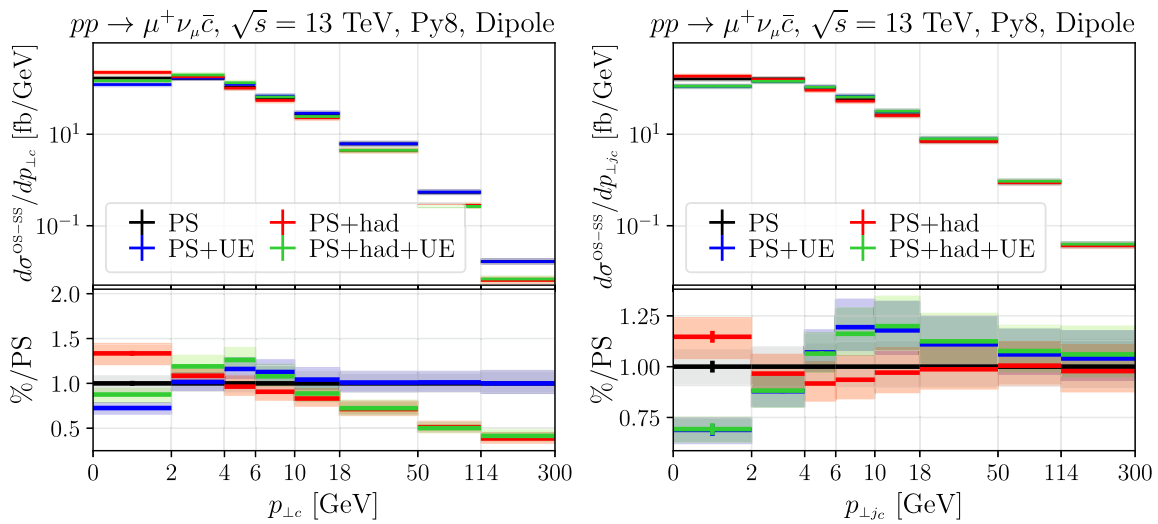


Fig. 10 Same as Fig. 9, but for the Pythia8.3 Dipole shower

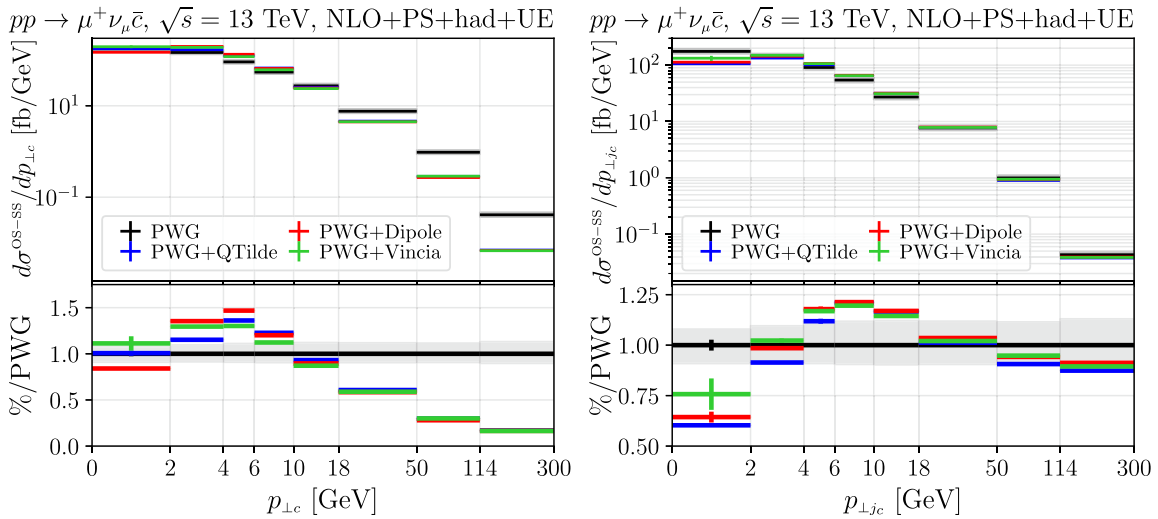


Fig. 11 Same as Fig. 8, but NLO + PS simulations have been supplemented with the underlying-event activity and the hadronization

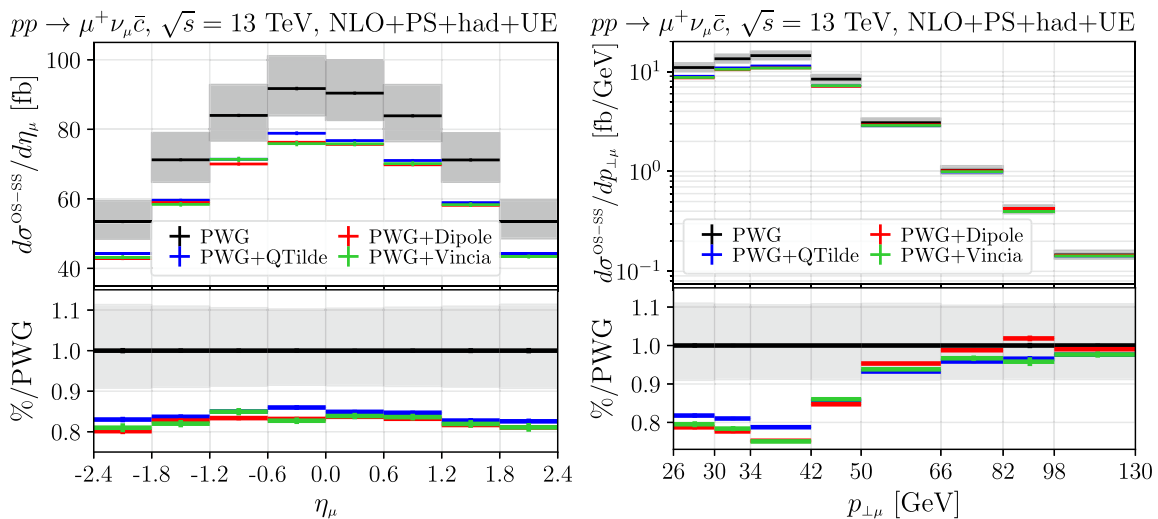


Fig. 12 Same as Fig. 11 for the muon pseudo-rapidity (left) and transverse momentum (right), and using the cuts in Eq. (4.1)

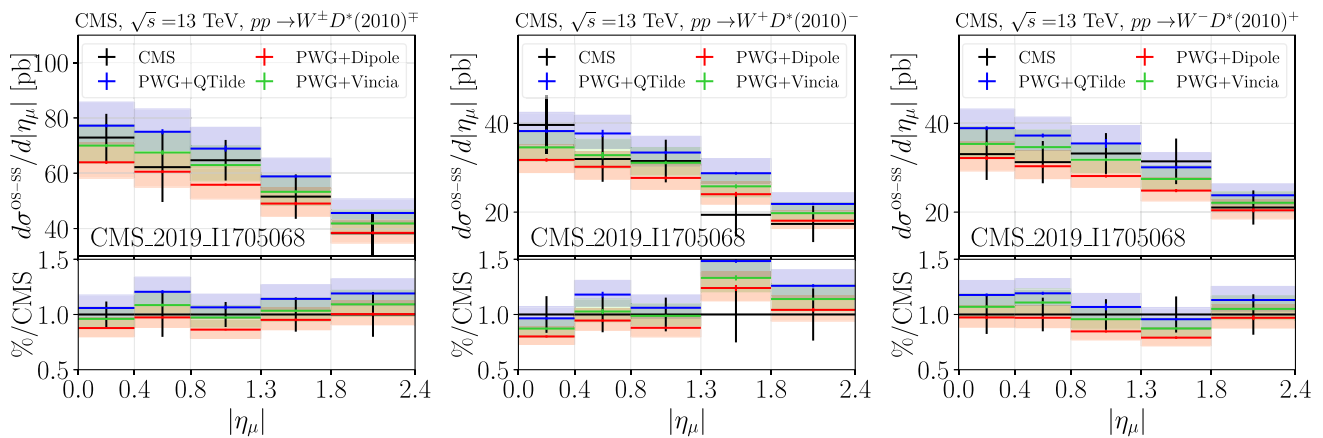


Fig. 13 Muon pseudo-rapidity in $pp \rightarrow WD^*$ events at $\sqrt{s} = 13$ TeV, using the selection cuts of the CMS analysis of Ref. [6], which are implemented in the Rivet analysis CMS_2019_I1705068. The experimental data and their combined statistical and systematic errors are drawn in black. The particle-level results obtained interfacing the POWHEG BOX

RES with the Herwig7.2 (QTilde, in blue) and the Pythia8.3 showers (Dipole, in red, and Vincia, in green) are also shown together with their scale-uncertainty bands, produced by varying μ_F and μ_R in the PWG calculation, performing the 7-point scale variations of Eq. (2.12)

In Fig. 12 we plot the pseudo-rapidity¹² (left panel) and the transverse momentum (right panel) of the muon, after applying the cuts in Eq. (4.1). Leptonic distributions are indirectly affected by the shower, that induces a modification of the momenta of the charmed quarks/hadrons. In particular, the softening of the charm quarks induced by the hadronization reduces the cross section. This reduction is clearly visible on the left panel of Fig. 12, with an almost uniform reduction of the cross section in the whole pseudo-rapidity range, of roughly 15%, with respect to the LHE result. In addition, all the three shower results are in very good agreement with each others. As far as the transverse momentum of the muon is concerned, shown on the right panel, we observe a significant shape variation as the bulk of the distribution, peaked around $p_{\perp\mu} \approx m_W/2$, gets depleted. Differences among the three showers amount to few percents, and are much smaller than the scale-variation band.

4.3 Comparison with the CMS data

In this section we compare our results against the CMS measurements at $\sqrt{s} = 13$ TeV for the associated production of a W boson and a charm quark [6]. The W boson is identified from its decay products: only events with a muon with $p_{\perp\mu} > 26$ GeV and $|\eta_\mu| < 2.4$ are selected. The charm quarks are tagged by reconstructing the $D^*(2010)$ mesons, which are required to have $p_{\perp D^*} > 5$ GeV and $|\eta_{D^*}| < 2.4$.¹³

¹² We remind the reader that since we include lepton-mass effects when generating events, as described in Sect. 2.3, the rapidity and pseudo-rapidity of the leptons differ.

¹³ These cuts correspond to the ones we have used in Sect. 4.2, with the exception that here no cut on $m_{\tau W}$ is imposed.

The background arising from $g \rightarrow c\bar{c}$ splitting is removed subtracting contributions where the charge of the resolved D^* meson and the muon have the same sign, as described in Sect. 4.2. We employ the Rivet3 [51] plugin to analyze the events generated by our simulations. Since the W boson is reconstructed from dressed leptons, in this case we also include the effect of the QED shower. All the other parameters are identical to those presented in Sect. 4.2.

The results of our comparison are illustrated in Fig. 13 for the inclusive $W^\mp D^*(2010)^\pm$ process, on the left panel, for $W^+ D^*(2010)^-$, on the middle panel, and for the $W^- D^*(2010)^+$ signature, on the right panel. Among all the showers, Vincia seems to be following the data more closely, slightly underestimating them, in the default Pythia8.3 configuration, while the Herwig7.2 results do instead lead to a larger value of the cross section. We notice that the Dipole shower distributions showed here are very similar to the ones presented in Ref. [12], where different PDF sets and tunes were employed. We want however to stress that we use the default tune of the showers, and this distribution is particularly sensitive to the hadronization modelling. For example, the Herwig7.2 hadronization parameters have been tuned in Ref. [52] using LEP data at the Z mass. Due to the fact that B mesons primarily decay into D ones, the charm hadronization is further affected by its interplay with the bottom hadronization. Thus, a dedicated tune will certainly allow for a better comparison with the data.

5 Conclusions

In this article we have presented the implementation of a NLO + parton-shower generator for massive-charm produc-

tion in association with a leptonically-decaying W boson in hadron collisions in the POWHEG BOX RES framework. This process is particularly crucial for the determination of the strange-quark content of the proton.

All spin-correlation effects and off-shell contributions in the W decay are properly included, and also non-diagonal elements in the Cabibbo–Kobayashi–Maskawa matrix.

The leading-order and the one-loop matrix elements have been computed analytically, allowing for a very fast and numerically-stable evaluation of the amplitudes.

Using the flexibility of the POWHEG method on the possibility to separate the real-radiation contribution into a finite and a divergent part, that is then exponentiated in the Sudakov form factor, we have implemented different ways to separate the real term and assessed the sensitivity of several kinematic distributions to this extra degree of freedom.

The main source of theoretical uncertainty remains the dependence on the factorization and renormalization scales, of the order of 10% for most kinematic distributions.

Events generated with our code have been interfaced with the Herwig7.2 QTilde shower, as well with the Pythia8.3 default shower and the Vincia one. We have investigated the effect of the parton shower, hadronization and of the underlying-event activity on several kinematic distributions. In particular hadronization corrections turned out to have the highest impact on the differential cross sections.

Particle-level results obtained with the three shower models we have used agree very well with each other, once hadronization corrections and the underlying-event simulation are also included.

Finally we compared our results with the CMS data for the WD^* signature, finding good agreement, within the scale-variation bands.

Acknowledgements The fixed order NLO part of the code we have presented in this paper was computed and implemented during S.F.R.'s Master thesis project. S.F.R. wants to acknowledge her co-advisors Federico Granata and Paolo Nason for guidance during the implementation of the project. S.F.R. also wants to thank Rob Verheyen for fruitful discussions on the Vincia shower. S.F.R. and C.O. thank Katerina Lipka for useful clarifications concerning the CMS Rivet analysis, and Tomáš Ježo and Alexander Huss for useful comments on the manuscript.

Data Availability Statement This manuscript has no associated data or the data will not be deposited. [Authors' comment: The datasets generated during and/or analysed during the current study are available from the corresponding author on reasonable request.]

Open Access This article is licensed under a Creative Commons Attribution 4.0 International License, which permits use, sharing, adaptation, distribution and reproduction in any medium or format, as long as you give appropriate credit to the original author(s) and the source, provide a link to the Creative Commons licence, and indicate if changes were made. The images or other third party material in this article are included in the article's Creative Commons licence, unless indicated otherwise in a credit line to the material. If material is not included in the article's Creative Commons licence and your intended

use is not permitted by statutory regulation or exceeds the permitted use, you will need to obtain permission directly from the copyright holder. To view a copy of this licence, visit <http://creativecommons.org/licenses/by/4.0/>.

Funded by SCOAP³. SCOAP³ supports the goals of the International Year of Basic Sciences for Sustainable Development.

References

1. U. Baur, F. Halzen, S. Keller, M.L. Mangano, K. Riesselmann, The Charm content of $W + 1$ jet events as a probe of the strange quark distribution function. *Phys. Lett. B* **318**, 544–548 (1993). [https://doi.org/10.1016/0370-2693\(93\)91553-Y](https://doi.org/10.1016/0370-2693(93)91553-Y). [arXiv:hep-ph/9308370](https://arxiv.org/abs/hep-ph/9308370)
2. ATLAS collaboration, G. Aad et al., Measurement of the production of a W boson in association with a charm quark in pp collisions at $\sqrt{s} = 7$ TeV with the ATLAS detector. *JHEP* **05**, 068 (2014). [https://doi.org/10.1007/JHEP05\(2014\)068](https://doi.org/10.1007/JHEP05(2014)068). [arXiv:1402.6263](https://arxiv.org/abs/1402.6263)
3. ATLAS collaboration, Measurement of the production of a W boson in association with a charmed hadron in pp collisions at $\sqrt{s} = 13$ TeV with the ATLAS detector. [arXiv:2302.00336](https://arxiv.org/abs/2302.00336)
4. CMS collaboration, S. Chatrchyan et al., Measurement of associated $W +$ charm Production in pp collisions at $\sqrt{s} = 7$ TeV. *JHEP* **02**, 013 (2014). [https://doi.org/10.1007/JHEP02\(2014\)013](https://doi.org/10.1007/JHEP02(2014)013). [arXiv:1310.1138](https://arxiv.org/abs/1310.1138)
5. CMS collaboration, A. Tumasyan et al., Measurements of the associated production of a W boson and a charm quark in proton–proton collisions at $\sqrt{s} = 8$ TeV. *Eur. Phys. J. C* **82**, 1094 (2022). <https://doi.org/10.1140/epjc/s10052-022-10897-7>. [arXiv:2112.00895](https://arxiv.org/abs/2112.00895)
6. CMS collaboration, A.M. Sirunyan et al., Measurement of associated production of a W boson and a charm quark in proton–proton collisions at $\sqrt{s} = 13$ TeV. *Eur. Phys. J. C* **79**, 269 (2019). <https://doi.org/10.1140/epjc/s10052-019-6752-1>. [arXiv:1811.10021](https://arxiv.org/abs/1811.10021)
7. LHCb collaboration, R. Aaij et al., Study of W boson production in association with beauty and charm. *Phys. Rev. D* **92**, 052001 (2015). <https://doi.org/10.1103/PhysRevD.92.052001>. [arXiv:1505.04051](https://arxiv.org/abs/1505.04051)
8. W.T. Giele, S. Keller, E. Laenen, QCD corrections to W boson plus heavy quark production at the Tevatron. *Phys. Lett. B* **372**, 141–149 (1996). [https://doi.org/10.1016/0370-2693\(96\)00078-0](https://doi.org/10.1016/0370-2693(96)00078-0). [arXiv:hep-ph/9511449](https://arxiv.org/abs/hep-ph/9511449)
9. W.J. Stirling, E. Vryonidou, Charm production in association with an electroweak gauge boson at the LHC. *Phys. Rev. Lett.* **109**, 082002 (2012). <https://doi.org/10.1103/PhysRevLett.109.082002>. [arXiv:1203.6781](https://arxiv.org/abs/1203.6781)
10. M. Czakon, A. Mitov, M. Pellen, R. Poncelet, NNLO QCD predictions for $W+c$ -jet production at the LHC. *JHEP* **06**, 100 (2021). [https://doi.org/10.1007/JHEP06\(2021\)100](https://doi.org/10.1007/JHEP06(2021)100). [arXiv:2011.01011](https://arxiv.org/abs/2011.01011)
11. M. Czakon, A. Mitov, M. Pellen, R. Poncelet, A detailed investigation of $W+c$ -jet at the LHC. *JHEP* **02**, 241 (2023). [https://doi.org/10.1007/JHEP02\(2023\)241](https://doi.org/10.1007/JHEP02(2023)241). [arXiv:2212.00467](https://arxiv.org/abs/2212.00467)
12. G. Bevilacqua, M. V. Garzelli, A. Kardos, L. Toth, $W+c$ charm production with massive c quarks in PowHel. *JHEP* **04**, 056 (2022). [https://doi.org/10.1007/JHEP04\(2022\)056](https://doi.org/10.1007/JHEP04(2022)056). <https://arxiv.org/abs/2106.11261>
13. P. Nason, A new method for combining NLO QCD with shower Monte Carlo algorithms. *JHEP* **11**, 040 (2004). <https://doi.org/10.1088/1126-6708/2004/11/040>. [arXiv:hep-ph/0409146](https://arxiv.org/abs/hep-ph/0409146)
14. S. Frixione, B.R. Webber, Matching NLO QCD computations and parton shower simulations. *JHEP* **06**, 029 (2002). <https://doi.org/10.1088/1126-6708/2002/06/029>. [arXiv:hep-ph/0204244](https://arxiv.org/abs/hep-ph/0204244)
15. J. Alwall, R. Frederix, S. Frixione, V. Hirschi, F. Maltoni, O. Mattelaer et al., The automated computation of tree-level and next-to-leading order differential cross sections, and their matching to parton shower simulations. *JHEP* **07**, 079 (2014). [https://doi.org/10.1007/JHEP07\(2014\)079](https://doi.org/10.1007/JHEP07(2014)079). [arXiv:1405.0301](https://arxiv.org/abs/1405.0301)

16. P. Nason, C. Oleari, M. Rocco, M. Zaro, An interface between the POWHEG BOX and MadGraph5_aMC@NLO. *Eur. Phys. J. C* **80**, 985 (2020). <https://doi.org/10.1140/epjc/s10052-020-08559-9>. arXiv:2008.06364
17. S. Frixione, P. Nason, C. Oleari, Matching NLO QCD computations with Parton Shower simulations: the POWHEG method. *JHEP* **11**, 070 (2007). <https://doi.org/10.1088/1126-6708/2007/11/070>. arXiv:0709.2092
18. S. Alioli, P. Nason, C. Oleari, E. Re, A general framework for implementing NLO calculations in shower Monte Carlo programs: the POWHEG BOX. *JHEP* **06**, 043 (2010). [https://doi.org/10.1007/JHEP06\(2010\)043](https://doi.org/10.1007/JHEP06(2010)043). arXiv:1002.2581
19. T. Ježo, P. Nason, On the treatment of resonances in next-to-leading order calculations matched to a parton shower. *JHEP* **12**, 065 (2015). [https://doi.org/10.1007/JHEP12\(2015\)065](https://doi.org/10.1007/JHEP12(2015)065). arXiv:1509.09071
20. L. Barze, G. Montagna, P. Nason, O. Nicrosini, F. Piccinini, Implementation of electroweak corrections in the POWHEG BOX: single W production. *JHEP* **04**, 037 (2012). [https://doi.org/10.1007/JHEP04\(2012\)037](https://doi.org/10.1007/JHEP04(2012)037). arXiv:1202.0465
21. J. Mazzitelli, P.F. Monni, P. Nason, E. Re, M. Wiesemann, G. Zanderighi, Next-to-next-to-leading order event generation for top-quark pair production. *Phys. Rev. Lett.* **127**, 062001 (2021). <https://doi.org/10.1103/PhysRevLett.127.062001>. arXiv:2012.14267
22. J. Mazzitelli, P.F. Monni, P. Nason, E. Re, M. Wiesemann, G. Zanderighi, Top-pair production at the LHC with MINNLO_{PS}. *JHEP* **04**, 079 (2022). [https://doi.org/10.1007/JHEP04\(2022\)079](https://doi.org/10.1007/JHEP04(2022)079). arXiv:2112.12135
23. S. Zanolì, M. Chiesa, E. Re, M. Wiesemann, G. Zanderighi, Next-to-next-to-leading order event generation for VH production with $H \rightarrow b\bar{b}$ decay. *JHEP* **07**, 008 (2022). [https://doi.org/10.1007/JHEP07\(2022\)008](https://doi.org/10.1007/JHEP07(2022)008). arXiv:2112.04168
24. A. Gavardi, C. Oleari, E. Re, NNLO+PS Monte Carlo simulation of photon pair production with MINNLO_{PS}. *JHEP* **09**, 061 (2022). [https://doi.org/10.1007/JHEP09\(2022\)061](https://doi.org/10.1007/JHEP09(2022)061). arXiv:2204.12602
25. P.F. Monni, P. Nason, E. Re, M. Wiesemann, G. Zanderighi, MiNNLO_{PS}: a new method to match NNLO QCD to parton showers. *JHEP* **05**, 143 (2020). [https://doi.org/10.1007/JHEP05\(2020\)143](https://doi.org/10.1007/JHEP05(2020)143). arXiv:1908.06987
26. P.F. Monni, E. Re, M. Wiesemann, MiNNLO_{PS}: optimizing $2 \rightarrow 1$ hadronic processes. *Eur. Phys. J. C* **80**, 1075 (2020). <https://doi.org/10.1140/epjc/s10052-020-08658-5>. arXiv:2006.04133
27. G. Cullen et al., GOSAM-2.0: a tool for automated one-loop calculations within the Standard Model and beyond. *Eur. Phys. J. C* **74**, 3001 (2014). <https://doi.org/10.1140/epjc/s10052-014-3001-5>. arXiv:1404.7096
28. G. Cullen, N. Greiner, G. Heinrich, G. Luisoni, P. Mastrolia, G. Ossola et al., Automated one-loop calculations with GoSam. *Eur. Phys. J. C* **72**, 1889 (2012). <https://doi.org/10.1140/epjc/s10052-012-1889-1>. arXiv:1111.2034
29. J. Alwall, P. Demin, S. de Visscher, R. Frederix, M. Herquet, F. Maltoni et al., MadGraph/MadEvent v4: the new web generation. *JHEP* **09**, 028 (2007). <https://doi.org/10.1088/1126-6708/2007/09/028>. arXiv:0706.2334
30. J.M. Campbell, R.K. Ellis, R. Frederix, P. Nason, C. Oleari, C. Williams, NLO Higgs boson production plus one and two jets using the POWHEG BOX, MadGraph4 and MCFM. *JHEP* **07**, 092 (2012). [https://doi.org/10.1007/JHEP07\(2012\)092](https://doi.org/10.1007/JHEP07(2012)092). arXiv:1202.5475
31. J.C. Collins, F. Wilczek, A. Zee, Low-energy manifestations of heavy particles: application to the neutral current. *Phys. Rev. D* **18**, 242 (1978). <https://doi.org/10.1103/PhysRevD.18.242>
32. T. Appelquist, J. Carazzone, Infrared singularities and massive fields. *Phys. Rev. D* **11**, 2856 (1975). <https://doi.org/10.1103/PhysRevD.11.2856>
33. M. Cacciari, M. Greco, P. Nason, The p_T spectrum in heavy flavor hadroproduction. *JHEP* **05**, 007 (1998). <https://doi.org/10.1088/1126-6708/1998/05/007>. arXiv:hep-ph/9803400
34. G. Luisoni, C. Oleari, F. Tramontano, $Wb\bar{b}j$ production at NLO with POWHEG+MiNLO. *JHEP* **04**, 161 (2015). [https://doi.org/10.1007/JHEP04\(2015\)161](https://doi.org/10.1007/JHEP04(2015)161). arXiv:1502.01213
35. A. Buckley, J. Ferrando, S. Lloyd, K. Nordström, B. Page, M. Rüfenacht et al., LHAPDF6: parton density access in the LHC precision era. *Eur. Phys. J. C* **75**, 132 (2015). <https://doi.org/10.1140/epjc/s10052-015-3318-8>. arXiv:1412.7420
36. NNPDF collaboration, R.D. Ball et al., Parton distributions from high-precision collider data. *Eur. Phys. J. C* **77**, 663 (2017). <https://doi.org/10.1140/epjc/s10052-017-5199-5>. arXiv:1706.00428
37. J. Campbell, T. Neumann, Precision phenomenology with MCFM. *JHEP* **12**, 034 (2019). [https://doi.org/10.1007/JHEP12\(2019\)034](https://doi.org/10.1007/JHEP12(2019)034). arXiv:1909.09117
38. J.M. Campbell, R.K. Ellis, W.T. Giele, A multi-threaded version of MCFM. *Eur. Phys. J. C* **75**, 246 (2015). <https://doi.org/10.1140/epjc/s10052-015-3461-2>. arXiv:1503.06182
39. J. Bellm, G. Nail, S. Plätzer, P. Schichtel, A. Siódmok, Parton shower uncertainties with Herwig 7: benchmarks at leading order. *Eur. Phys. J. C* **76**, 665 (2016). <https://doi.org/10.1140/epjc/s10052-016-4506-x>. arXiv:1605.01338
40. M. Cacciari, G.P. Salam, G. Soyez, FastJet user manual. *Eur. Phys. J. C* **72**, 1896 (2012). <https://doi.org/10.1140/epjc/s10052-012-1896-2>. arXiv:1111.6097
41. M. Cacciari, G.P. Salam, G. Soyez, The anti- k_r jet clustering algorithm. *JHEP* **04**, 063 (2008). <https://doi.org/10.1088/1126-6708/2008/04/063>. arXiv:0802.1189
42. A. Banfi, G.P. Salam, G. Zanderighi, Infrared safe definition of jet flavor. *Eur. Phys. J. C* **47**, 113–124 (2006). <https://doi.org/10.1140/epjc/s2006-02552-4>. arXiv:hep-ph/0601139
43. M. Bahr et al., Herwig++ physics and manual. *Eur. Phys. J. C* **58**, 639–707 (2008). <https://doi.org/10.1140/epjc/s10052-008-0798-9>. arXiv:0803.0883
44. J. Bellm et al., Herwig 7.2 release note. *Eur. Phys. J. C* **80**, 452 (2020). <https://doi.org/10.1140/epjc/s10052-020-8011-x>. arXiv:1912.06509
45. T. Sjöstrand, S. Mrenna, P.Z. Skands, PYTHIA 6.4 physics and manual. *JHEP* **05**, 026 (2006). <https://doi.org/10.1088/1126-6708/2006/05/026>. arXiv:hep-ph/0603175
46. T. Sjöstrand, S. Ask, J.R. Christiansen, R. Corke, N. Desai, P. Ilten et al., An introduction to PYTHIA 8.2. *Comput. Phys. Commun.* **191**, 159–177 (2015). <https://doi.org/10.1016/j.cpc.2015.01.024>. arXiv:1410.3012
47. B. Cabouat, T. Sjöstrand, Some dipole shower studies. *Eur. Phys. J. C* **78**, 226 (2018). <https://doi.org/10.1140/epjc/s10052-018-5645-z>. arXiv:1710.00391
48. H. Brooks, C.T. Preuss, P. Skands, Sector showers for hadron collisions. *JHEP* **07**, 032 (2020). [https://doi.org/10.1007/JHEP07\(2020\)032](https://doi.org/10.1007/JHEP07(2020)032). arXiv:2003.00702
49. P. Skands, R. Verheyen, Multipole photon radiation in the Vincia parton shower. *Phys. Lett. B* **811**, 135878 (2020). <https://doi.org/10.1016/j.physletb.2020.135878>. arXiv:2002.04939
50. S. Catani, B.R. Webber, G. Marchesini, QCD coherent branching and semiinclusive processes at large x. *Nucl. Phys. B* **349**, 635–654 (1991). [https://doi.org/10.1016/0550-3213\(91\)90390-J](https://doi.org/10.1016/0550-3213(91)90390-J)
51. C. Bierlich et al., Robust independent validation of experiment and theory: rivet version 3. *SciPost Phys.* **8**, 026 (2020). <https://doi.org/10.21468/SciPostPhys.8.2.026>. arXiv:1912.05451
52. G. Bewick, S. Ferrario Ravasio, P. Richardson, M.H. Seymour, Logarithmic accuracy of angular-ordered parton showers. *JHEP* **04**, 019 (2020). [https://doi.org/10.1007/JHEP04\(2020\)019](https://doi.org/10.1007/JHEP04(2020)019). arXiv:1904.11866